PNAS RESEARCH ARTICLE | ENGINEERING MEDICAL SCIENCES OPEN ACCESS

Throughput-scalable manufacturing of SARS-CoV-2 mRNA lipid nanoparticle vaccines

Sarah J. Shepherd[a], Xuexiang Han[a], Alvin J. Mukalel[a], Rakan El-Mayta[a], Ajay S. Thatte[a], Jingyu Wu[b], Marshall S. Padilla[a], Mohamad-Gabriel Alameh[c], Neha Srikumar[d], Daeyeon Lee[b], Drew Weissman[c], David Issadore[a,b,e,1], and Michael J. Mitchell[a,f,g,h,i,j,1,2]

Edited by David Weitz, Harvard University, Cambridge, MA; received March 2, 2023; accepted July 11, 2023

Lipid nanoparticles (LNPs) are a potent delivery technology that have made it possible for the recent clinical breakthroughs in mRNA therapeutics and vaccines. A key challenge to the broader implementation of mRNA therapeutics and vaccines is the development of technology to produce precisely defined LNP formulations, with throughput that can scale from discovery to commercial manufacturing and meet the stringent manufacturing standards of the pharmaceutical industry. To address these challenges, we have developed a microfluidic chip that incorporates 1×, 10×, or 256× LNP-generating units that achieve scalable production rates of up to 17 L/h of precisely defined LNPs. Using these chips, we demonstrate that LNP physical properties and potency in vivo are unchanged as throughput is scaled. Our chips are fabricated out of silicon and glass substrates, which have excellent solvent compatibility, compatibility with pharmaceutical manufacturing, and can be fully reset and reused. SARS-CoV-2 mRNA-LNP vaccines formulated by our chips triggered potent antibody responses in a preclinical study. These results demonstrate the feasibility of directly translating microfluidic-generated LNPs to the scale necessary for commercial production.

nanoparticle | nanomedicine | vaccines | drug delivery | mRNA

Significance

A major unmet need in the advancement of lipid nanoparticles (LNPs) for RNA therapeutics and vaccines is the development of formulation technologies that can generate LNPs across the various scales of drug development, from small-scale discovery experiments to large-scale clinical trials. Microfluidic technologies, which formulate LNPs with precisely defined properties, have been limited by scalability challenges. To overcome this, we fabricated a silicon and glass microfluidic platform for throughput-scalable manufacturing of mRNA-LNP vaccines. This technology can be widely applied to nanoparticle formulations and can accelerate the development of LNP-based RNA therapeutics and vaccines to address emerging pathogens and sudden outbreaks.

mRNA-based therapeutics and vaccines are revolutionizing the pharmaceutical industry as they provide unprecedented opportunities for protein replacement therapies, gene editing, and rapid vaccine development (1, 2). However, mRNAs are subject to rapid degradation and cannot achieve effective cellular uptake due to their large size and anionic charge; (3, 4) thus, they require a delivery platform for intracellular delivery to the target site. Ionizable lipid nanoparticles (LNPs) are a clinically translatable synthetic delivery vehicle for RNAs that are typically composed of an ionizable lipid, phospholipid, cholesterol, and a polyethylene glycol–lipid conjugate (PEG–lipid), where the ionizable lipid is neutrally charged at physiological pH and becomes charged in the acidic endosome so it can release the RNA cargo into the cytosol (5–7). Due to the self-assembly of the lipids and their electrostatic interactions with RNA, LNPs stabilize the nucleic acid cargo, minimize toxicity, and protect RNA from nuclease degradation (8, 9).

Notably, LNPs have been approved by the US Food and Drug Administration for severe acute respiratory syndrome coronavirus 2 (SARS-CoV-2) mRNA vaccines, which were developed by Moderna and Pfizer/BioNTech. In addition, they have been approved for the treatment of polyneuropathy by a small interfering RNA (siRNA) LNP as developed by Alnylam Pharmaceuticals (10, 11). For a given application, the LNP formulation parameters are optimized in small-scale discovery experiments to enhance RNA delivery by modifying the lipid chemical structures, mRNA modifications, or relative amounts of lipid and nucleic acid components (5, 12–14). However, once this optimized LNP formulation is identified, it can be challenging to produce this formulation at the high production rates needed for clinical testing and commercial production since the current methods for small-scale production and large-scale production differ (15, 16). Small-scale LNP production relies on pipette mixing or microfluidic mixing techniques (17, 18), while large-scale production uses T-junction mixing (16), a method of turbulent mixing where two input streams collide in a T-shaped mixing design. This challenge in scale-up can become costly with respect to time to ensure that LNP physical properties and potency are unchanged between formulation methods. In the case of outbreaks or pandemics, it is essential to minimize the time between the discovery phase and commercial production. During the coronavirus disease 2019 (COVID-19) pandemic, caused by SARS-CoV-2, there was an unprecedented need to develop a potent vaccine that could be manufactured at high volumes (19, 20). Among the vaccines that entered clinical trials, mRNA vaccines were a promising candidate since they facilitated a strong immune response and the mRNA could be synthesized rapidly without the need for cell cultures (21). However, throughout

Author contributions: S.J.S., D.I., and M.J.M. designed research; S.J.S., X.H., A.J.M., R.E.-M., A.S.T., J.W., M.S.P., M.-G.A., and N.S. performed research; S.J.S., X.H., M.S.P., M.-G.A., D.W., D.I., and M.J.M. contributed new reagents/analytic tools; S.J.S., X.H., D.I., and M.J.M. analyzed data; and S.J.S., X.H., D.L., D.I., and M.J.M. wrote the paper.

Competing interest statement: D.I. is a founder and holds equity in Infini Fluidics. D.W. is an inventor on several patents related to this work filed by the Trustees of the University of Pennsylvania (11/990,646; 13/585,517; 13/839,023; 13/839,155; 14/456,302; 15/339,363; and 16/299,202).

This article is a PNAS Direct Submission.

[1]D.I. and M.J.M. contributed equally to this work.

[2]To whom correspondence may be addressed. Email: mjmitch@seas.upenn.edu.

This article contains supporting information online at https://www.pnas.org/lookup/suppl/doi:10.1073/pnas.2303567120/-/DCSupplemental.

Published August 9, 2023.

the entire mRNA LNP production process, the LNP formulation method was identified as the bottleneck (21, 22) since companies operated multiple T-junction mixers simultaneously instead of engineering new mixing processes, which would have slowed down the rollout of vaccines (15). While this approach was sufficient to produce LNPs for the SARS-CoV-2 mRNA vaccines, there is an unmet need for scalable production processes to rapidly formulate nanomedicines to prevent future bottlenecks for upcoming LNP-based RNA therapeutic and vaccine applications.

Microfluidic chips—which facilitate millisecond mixing at the nanoliter scale—have been applied to LNP production to improve RNA encapsulation efficiency, reduce size heterogeneity, and ultimately produce more potent LNPs for mRNA therapeutics and vaccines (17, 23, 24). In contrast to traditional methods that involve lipid film hydration or bulk mixing that may require specialized infrastructure for downstream processing to reduce LNP size and size heterogeneity, microfluidic processes are robust and reproducible, as LNPs can be formulated with defined sizes by adjusting operating parameters, such as flow rates and flow rate ratios (25). While several microfluidic mixing architectures have been investigated, (26–29) staggered herringbone micromixers have emerged as a widely applied strategy due to short mixing times of <10 ms with smallest reported LNP sizes (<30 nm) (16, 17, 24, 30). While these microfluidic approaches are advantageous to produce small scale (0.1 L/h) LNP formulations for rapid screening, they cannot produce LNPs at commercial scales; thus, parallelization of mixing channels has been employed to increase production rates (23, 31–33). However, these chips were fabricated in polydimethylsiloxane (PDMS), which are incompatible with stringent pharmaceutical requirements due to sterility concerns and potential leaching of chip materials into the final product (34, 35). Additionally, other mixing architectures, such as bifurcating mixers, have been commercialized (Precision Nanosystems's NanoAssemblr platform) and can achieve high production rates of >10 L/h, but their approach is not easily scalable to >10× chips since each mixing unit requires macroscopic fluidic handling systems to each independent mixing chip (28). Currently, these microfluidic chips are not employed commercially due to remaining limitations in throughput and durability of chip operation—thus, other rapid mixing techniques, such as T-junction mixing, are used that cannot scale down to small-scale discovery experiments (15, 16).

Here, we present a silicon scalable lipid nanoparticle generation (SCALAR) platform fabricated entirely out of silicon and glass substrates that incorporates an array of 256 mixing units for high-throughput production of RNA LNPs on a single microfluidic chip (Fig. 1*B*). Our platform has the potential to shorten the time from LNP formulation optimization to clinical applications since our chips can achieve high production rates while minimizing variations in LNP physical properties or potency that could result from using differing formulation techniques at the small scale and large scale. Our design combines a ladder design geometry with branching architecture to incorporate 256 staggered herringbone micromixer mixing units onto a 100-mm silicon chip that can be operated at a moderate pressure of 100 pounds per square inch (PSI) and fabricated by conventional semiconductor processes (Fig. 1*C*). A ladder geometry is generally preferred for parallelized designs to distribute fluids to and collect fluids from individual mixing units since it requires a smaller footprint and is more resilient to clogging than a branched design alone (36) (*SI Appendix*, Fig. S1). Thus, we incorporated this design with a branched design for the inputs to reduce the operating pressure by 40%.

To ensure that each device in the array produces LNPs with identical physical parameters, we incorporated high fluidic resistance microchannels upstream of each device in the array to decouple the design of the mixing unit and the fluidics required for parallelization (39, 40). We fabricated chips that incorporated 1×, 10×, or 256× mixing units that allows the LNP production rate to be varied from 0.1 L/h to 17 L/h depending on the intended application without changing the mixing geometry or flow conditions compared to a single 1× mixing chip. Compared to previous microfluidic chips fabricated in polymers such as PDMS, our SCALAR chips are highly reproducible in fabrication and operation, are resistant to solvent swelling/damage, eliminate the concern for chip materials leaching into the product, and are compatible with high temperatures (T_{max} > 500 °C) required for sterilization processes such as autoclaving (41).

We used our SCALAR chips to formulate SARS-CoV-2 Spike-encoding mRNA LNP vaccines using a benchmark formulation (42) with FDA-approved DLin-MC3-DMA (MC3) as the ionizable lipid. We demonstrated similar LNP vaccine efficacy in mice, quantified by antigen-specific antibodies, following intramuscular administration of these LNPs formulated by standard PDMS microfluidic chips or our SCALAR chips. Further, we formulated LNPs at a production rate of 17 L/h, equivalent to 8.5 g/h mRNA or 34,000 vaccines doses per h (Fig. 1 *D* and *E*), demonstrating comparable LNP physical properties across all scales (1×, 10×, 256×) of the SCALAR chips. These results demonstrate the feasibility of silicon-glass microfluidic chips for large-scale and reproducible production of mRNA LNPs for therapeutic and vaccine applications. Additionally, our chip materials allow for the resetting and reuse of the chips. Since this fabrication strategy can parallelize many (>20,000) (43) identical microfluidic units, the total throughput can be scaled further by simply incorporating more mixing units on a single 100-mm microfluidic chip, thus eliminating the need for excess fluidic handling systems. Further, this LNP formulation process can be integrated with other processes (e.g., dialysis or tangential flow filtration) in a continuous manner to streamline RNA LNP production. The development of scalable microfluidics will enable LNP and nanomedicine therapies to become more widely exploited throughout the field as major manufacturing challenges are being addressed.

Results

Design and Fabrication of a Silicon and Glass Scale-Up Chip. All chips were fabricated using a single 500-μm thick 100-mm silicon wafer encapsulated in glass to increase production rates by over 200-fold compared to current small-scale single-channel microfluidic chips (24). By incorporating a ladder design architecture with branching instead of the ladder design alone, we reduced the operating pressure by 40% (100 PSI vs. 166 PSI) to ensure safe, reliable operation of the parallelized chip. Of note, these chips have a high maximum pressure (P_{max} > 1,000 PSI) afforded by anodic bonding. These design parameters, in combination with flow resistors, enabled the integration of 256 identical mixing units that used a well-validated staggered herringbone micromixer architecture (23, 24, 44) for the production of precisely defined, potent mRNA LNPs. In contrast to previous microfluidic approaches that have utilized polymeric substrates for chip construction, we chose to build our chips entirely out of silicon and glass to improve solvent compatibility, increase robustness of chip operation, and allow for a range of formulation conditions for future applications (e.g., high-temperature formulations, autoclaving for sterilization). We demonstrate that LNPs produced by our SCALAR chips match the potency of LNPs produced by the standard PDMS chip for mRNA delivery in vivo.

Our parallelized chip incorporates an array of 256 mixing units, where each mixing unit is connected to 1) layers of channels that

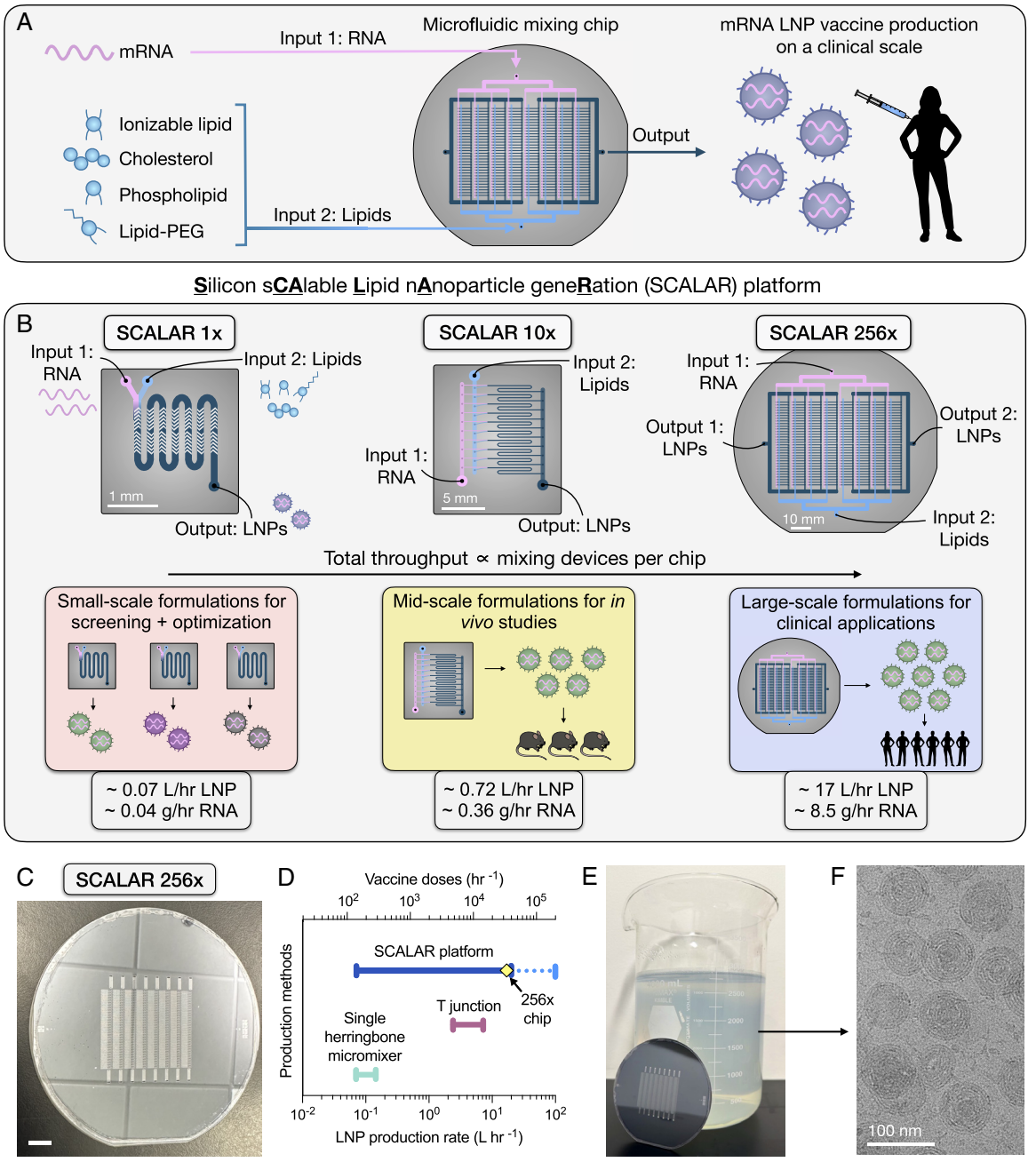

Fig. 1. Fabrication of a Silicon sCAlable Lipid nAnoparticle geneRation (SCALAR) platform for production of mRNA LNP vaccines. (*A*) Schematic for LNP formulation by rapid mixing of RNA and lipid components, where mRNA LNPs are generated on a scale relevant for clinical applications. (*B*) A throughput-scalable SCALAR platform that incorporates 1× (*Left*), 10× (*Center*), or 256× (*Right*) mixing units onto a single microfluidic chip to formulate mRNA LNPs for therapeutic and vaccine applications. Scale bars are 1 mm for the 1× chip; 5 mm for the 10× chip; 10 mm for the 256× chip. Relative volumetric throughputs and mass throughputs are shown for each chip with potential applications. (*C*) An image of the SCALAR 256× chip showing 256 mixing units. (Scale bar, 10 mm.) (*D*) Comparison of the LNP production rate for the SCALAR platform (*Top*; blue), T-junction mixing (37, 38) (*Center*; purple), and a single herringbone micromixer chip (23, 24) (*Bottom*; green) in terms of volumetric throughput (*Bottom x* axis) and mRNA vaccine doses per hour (*Top x* axis) assuming that 1 mRNA vaccine dose is equivalent to 0.5 mL LNP (= 0.1 mg mRNA). The blue dotted line for the SCALAR platform indicates what could be achieved with a 1000× chip. (*E*) Empty LNPs generated in 10 min by the 256× mixing chip (2.8 L) with the 256× chip in the foreground. (*F*) Cryo-TEM imaging of empty LNPs generated by the 256× mixing chip. (Scale bar, 100 nm.)

deliver the two inputs (RNA and lipids) and 2) layers of channels that collect the formulated LNPs. In our design, supply channels connect each external input to two branched sets of four delivery channel rows, totaling to eight rows. Each delivery channel row connects to 32 identical mixing units by vertical vias; each mixing unit consists of flow resistors upstream of staggered herringbone mixing channels (*SI Appendix*, Fig. S2). Finally, mixing units are connected to channels that deliver the formulated LNPs to external outputs by vertical vias. The silicon wafers are patterned with four steps of lithography and deep reactive ion etching—standard processes in microfabrication—to define the mixing channels (h = 70 μm), herringbones and resistors (h = 25 μm), vias (h = 60 μm), and delivery channels (h = 370 μm) (*SI Appendix*, Fig. S3). The patterned silicon wafer is anodically bonded to Borofloat glass wafers on each side to encapsulate the design; one of the glass wafers is micromachined with holes for the inputs and outputs prior to bonding to enable macroscopic fluidic connections. A custom chip holder machined out of 6061-T651 aluminum (manufactured by Protolabs)

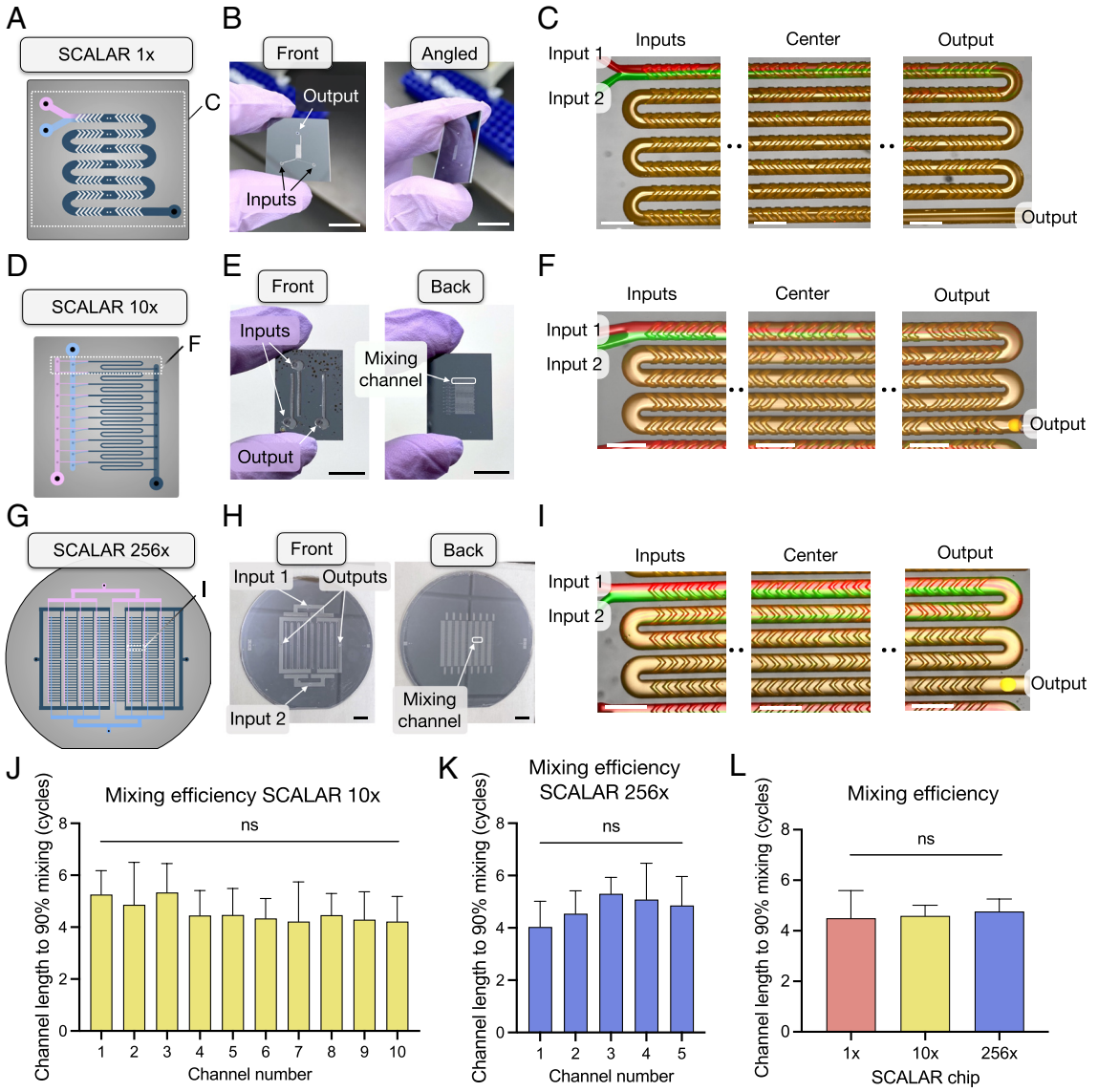

Fig. 2. Validation of device performance across all scales of SCALAR chips by mixing quantification. Fluorescein (FITC)–dextran and rhodamine B–dextran were flowed through each chip (1×, 10×, 256×) (*A*–*I*) to perform mixing analysis by quantifying mixing efficiency (*J*–*L*). (*A*–*C*) A single mixing chip (SCALAR 1×), showing a schematic of the chip (*A*), images of the chip (*B*), and fluorescent images (*C*) of mixing in a channel. (*D*–*F*) A single row parallelized chip (SCALAR 10×), showing a schematic of the chip (*D*), images of the chip (*E*), and fluorescent images (*F*) of mixing. (*G*–*I*) A parallelized chip (SCALAR 256×), showing a schematic of the chip (*G*), images of the chip (*H*), and fluorescent images (*I*) of mixing. (*J*–*L*) Quantification of mixing efficiency (±SD; errors produced by a curve-fitting model), calculated by the channel length needed for fluids to become 90% mixed. (*J*) Mixing efficiency for each of the 10 channels in the SCALAR 10× chip. Samples were compared by a one-way ANOVA. $P = 0.9096$. (*K*) Mixing efficiency for five channels in the SCALAR 256× chip, where the channels chosen surveyed the top left (channel 1), top right (channel 2), center (channel 3), bottom left (channel 4), and bottom right (channel 5) of the chip. Samples were compared by a one-way ANOVA. $P = 0.2634$. (*L*) Comparison of mixing efficiency for all scales of SCALAR chips. Samples were compared by a one-way ANOVA. $P = 0.3914$. Scale bars are 10 mm for the chip images (*B*, *E*, and *H*) and 300 μm for the fluorescent images (*C*, *F*, and *I*).

encased the chip, allowing for observation of mixing channels on the topside with threaded ports for the inputs and outputs on the backside of the holder (*SI Appendix*, Figs. S4 and S5). Reagents are delivered to the chip by a custom pressure-driven system, where stainless steel pressure vessels are pressurized with nitrogen and reagents are delivered to the chip by PTFE tubing and stainless steel fittings.

Our SCALAR platform includes chips that incorporate 1×, 10×, or 256× mixing units, where the mixing design is unchanged between chips, ensuring that each mixing unit at any scale of parallelization operates with the same flow conditions and thus produces identical LNPs for potent mRNA delivery. To ensure this, we followed previously established design rules for designing arrays of microfluidic droplet generators, (39–41) where each mixing unit has a much higher fluidic resistance than its upstream delivery channels; thus, the mixing units operate as if connected in parallel.

Chip Validation and Investigation of Reuse. To validate our design principles, we analyzed the mixing performance of SCALAR chips that incorporated 1× (Fig. 2 *A*–*C*), 10× (Fig. 2 *D*–*F* and *SI Appendix*, Fig. S6), or 256× (Fig. 2 *G*–*I* and *SI Appendix*, Fig. S7) mixing units. Two fluorescent dyes, fluorescein isothiocyanate (FITC) dextran and rhodamine B isothiocyanate dextran, were flowed through each chip, and images were captured and analyzed with image analysis software (ImageJ) to quantify a mixing value for positions throughout the channel. These dyes were selected since they approximate the size of our LNP components, such as the lipids and RNA (45, 46), respectively, and the fluorescent intensity profiles could be quantified by independent fluorescence channels. The mixing value ranged from 1 (not mixed) to 0 (completely mixed) as previously described, (32) where a mixing value of 0.1 indicated the channel length at which the dyes are 90% mixed—a

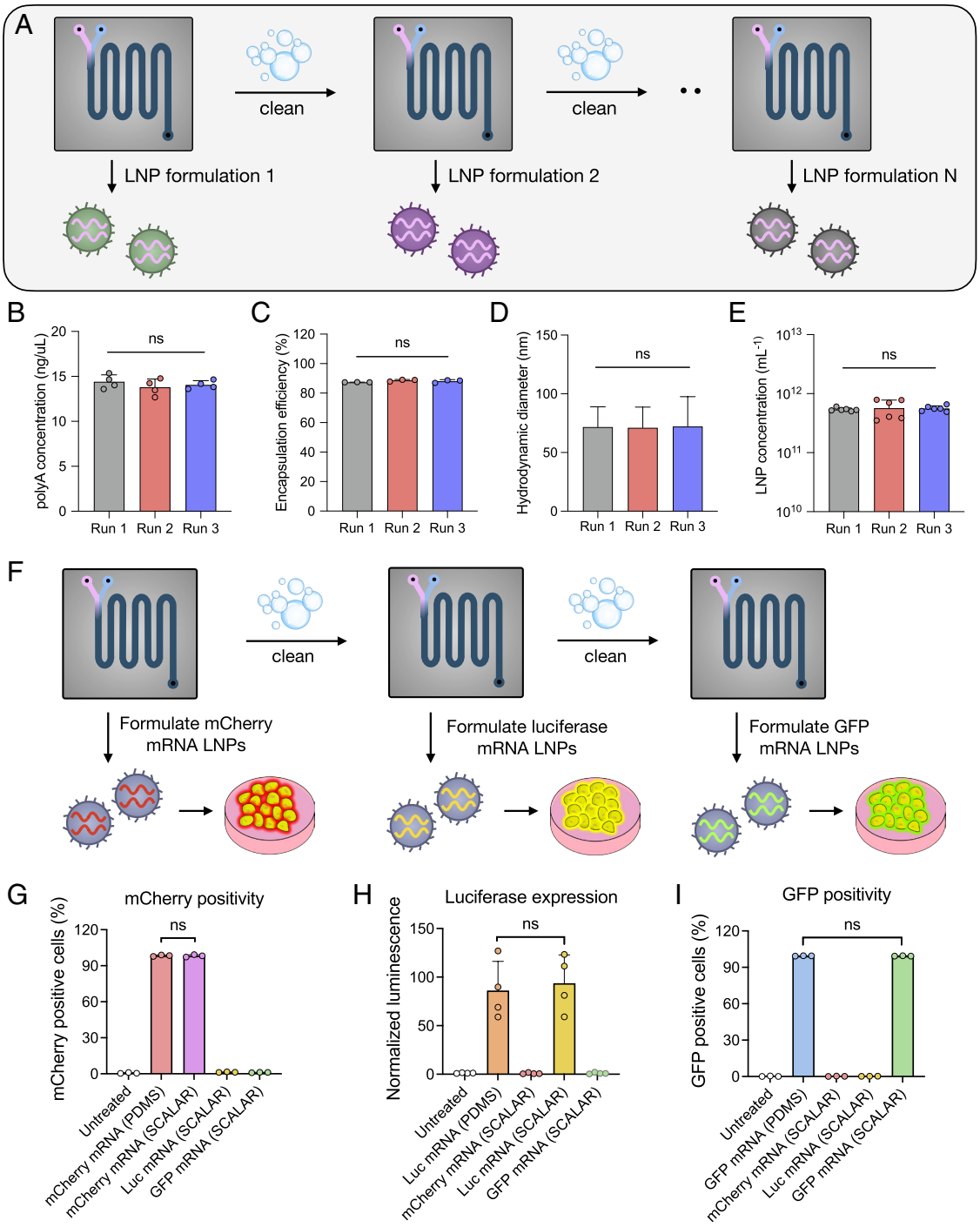

Fig. 3. SCALAR chips enhance the durability of chip operation by enabling chip reuse. (*A*) Schematic for experiment: LNPs were formulated in a single (SCALAR 1×) chip until the chip was fouled (~20 min); the chip was reset with Triton-X 100 surfactant prior to the next LNP formulation. (*B–E*) The same polyA LNP formulation was produced in three consecutive runs with the same microfluidic chip with no significant changes in LNP physical properties between runs. (*B*) PolyA concentration (±SD), quantified by a RiboGreen assay, from the LNPs produced. n = 4 technical replicates. Samples were compared by an ordinary one-way ANOVA, $P = 0.5245$. (*C*) PolyA encapsulation efficiency (±SD), quantified by a RiboGreen assay. n = 3 technical replicates. Samples were compared by an ordinary one-way ANOVA, $P = 0.1768$. (*D*) LNP diameter (±SD), quantified by intensity-based dynamic light scattering. Errors are calculated SD from the average size and PDI. n = 3 measurements. Samples were compared by an ordinary one-way ANOVA, $P = 0.9979$. (*E*) LNP concentration (±SD), quantified by a combination of dynamic and static light scattering. n = 6 measurements. Samples were compared by an ordinary one-way ANOVA, $P = 0.9177$. (*F*) Schematic for experiment: Three different mRNA LNP formulations were produced in the same single (SCALAR 1×) chip; the chip was cleaned with Triton-X 100 surfactant between formulations. (*G*) mCherry mRNA LNPs were formulated and administered to Jurkat cells at a dose of 60 ng/60,000 cells; mCherry expression was quantified by percent positive cells using flow cytometry at 24 h. n = 3 technical replicates. Samples were compared by the two-tailed unpaired *t* test; $P = 0.8438$. (*H*) Luciferase mRNA LNPs were formulated and administered to Jurkat cells at a dose of 60 ng/60,000 cells; luciferase expression was quantified by luminescence at 24 h. n = 4 technical replicates. Samples were compared by the two-tailed unpaired *t* test; $P = 0.7541$. (*I*) GFP mRNA LNPs were formulated and administered to Jurkat cells at a dose of 60 ng/60,000 cells; GFP expression was quantified by percent positive cells using flow cytometry at 24 h. n = 3 technical replicates. Samples were compared by two-tailed unpaired *t* test; $P = 0.6702$.

value that could be compared across chips. We determined that all scales of SCALAR chips had equal mixing efficiency, as determined by channel length needed for 90% mixing (Fig. 2 *J–L*).

Next, we investigated the reuse of SCALAR chips for RNA LNP formulations. For these studies, we used a single 1× mixing chip. We formulated LNPs with the ionizable lipid MC3, phospholipid

distearoylphosphatidylcholine (DSPC), cholesterol, and DMG-PEG 2000 to encapsulate polyA as a substitute for mRNA. PolyA was chosen as a substitute for mRNA due to its low cost, high encapsulation (>80%) in LNPs, and prior use in the field (25) for LNP formulations. It is well known that microfluidic chips can foul or clog over time (47, 48), a phenomenon that we observed in our mixing chips after ~20 min of LNP formulation (Fig. 3*A* and *SI Appendix*, Fig. S8). We used a nonionic surfactant (1% triton X 100) followed by a nitrogen purge to clean the chip after 20 min of polyA LNP formulation and repeated this process three times to compare LNP physical properties between the three runs (Fig. 3 *B*–*E* and *SI Appendix*, Fig. S9). Triton X was selected as a cleaning agent for the chip due to its use in LNP characterization assays (e.g., RiboGreen assay) to lyse LNPs. We found no significant differences in polyA concentration, relative encapsulation efficiency, LNP hydrodynamic diameter, or LNP concentration as measured by a RiboGreen fluorescent quantitation kit (polyA concentration, encapsulation), dynamic light scattering (size), or a combination of dynamic and static light scattering (LNP concentration). We confirmed that our cleaning method was effective in resetting these chips for a single LNP formulation with high repeatability. Additionally, we autoclaved a SCALAR 1× mixing chip and formulated luciferase mRNA LNPs before and after the autoclaving cycle to demonstrate the chip's compatibility with pharmaceutical regulations. Device performance was not affected by autoclaving; the formulated LNPs had no significant differences in physical properties or potency for mRNA delivery to HepG2 cells (*SI Appendix*, Fig. S10).

Further, we tested whether we could formulate LNPs with different compositions on the same mixing chip without compromising LNP potency or physical parameters. Using a single 1× chip, we formulated LNPs encapsulating mCherry-encoding mRNA, luciferase-encoding mRNA, or GFP-encoding mRNA and cleaned the chip between runs using the same protocol as described previously (Fig. 3*F* and *SI Appendix*, Fig. S11). We evaluated the potency of mRNA LNPs generated by a SCALAR 1× chip compared to a PDMS 1× chip and ensured that each LNP formulation was independent and did not contain mRNA LNPs from the previous formulation run. We delivered these mRNA LNPs to Jurkat cells, an immortalized T cell, and measured functional delivery of mRNA by luminescence or flow cytometry. We found no significant differences in the potency of mRNA LNPs from a standard PDMS 1× chip or a SCALAR 1× chip (Fig. 3 *G*–*I*) and did not detect any transfection from the mRNA LNPs generated in previous formulation runs, thus eliminating the concern for cross-contamination between subsequent formulations. Collectively, we validated the performance of our SCALAR platform (1×, 10×, or 256×) for rapid mixing and demonstrated its potential to be leveraged as a reusable mixing chip.

Formulation of LNPs for Potent mRNA Delivery In Vitro, Ex Vivo, and In Vivo. To validate that our SCALAR platform could formulate LNPs for potent mRNA delivery, we produced LNPs at two different scales (SCALAR 1×, 10×) and compared the physical properties to bulk mixed LNPs and LNPs generated by a standard PDMS 1× mixing chip. Additionally, we measured the potency of these luciferase-encoding mRNA LNPs by delivering them to HepG2 cells, primary T cells, or mice and quantified functional mRNA delivery by luminescence measurements. HepG2 cells were chosen since they are a common cell line for LNP screening (49). We used a SCALAR 10× chip in lieu of the SCALAR 256× chip for these studies to validate our parallelized design principles. Throughout this study, we demonstrate that LNP properties and potency are comparable between microfluidic formulations (SCALAR 1×, SCALAR 10×, PDMS 1×), which outperform bulk mixed LNPs for in vitro and ex vivo mRNA delivery.

We formulated LNPs with the ionizable lipid MC3, a well-validated ionizable lipid that has been FDA approved for Onpattro, (8) an RNA LNP therapeutic. We combined MC3 with the phospholipid DSPC, cholesterol, and lipid-anchored PEG (DMG-PEG 2000) for our mRNA formulations at a molar ratio of 50:10:38.5:1.5, respectively, similar to the Spikevax SARS-CoV-2 mRNA vaccine developed by Moderna. Cryo-TEM imaging of the mRNA LNPs demonstrated the polydispersity of bulk mixed LNPs with respect to size distribution and morphology (Fig. 4*A*) while the microfluidic-formulated LNPs (Fig. 4 *B*–*D* and *SI Appendix*, Fig. S12) were relatively monodisperse with respect to size distribution and had a uniform, electron-dense morphology. Dynamic light scattering revealed that there were no significant differences in the hydrodynamic size between SCALAR 1×-generated LNPs, SCALAR 10×-generated LNPs, and PDMS 1×-generated LNPs (approx. 70 nm), which were significantly smaller than bulk mixed LNPs (approx. 160 nm) (Fig. 4*E*). Relative encapsulation efficiency measurements, quantified by a RiboGreen assay, demonstrated that LNPs generated by microfluidic chips had a high relative encapsulation efficiency (>85%), while bulk mixed LNPs had a lower relative encapsulation efficiency (~60%) (Fig. 4*F*). We delivered these luciferase-encoding mRNA LNPs to HepG2 cells at a dose of 50 ng per 5k cells and found comparable potency between all methods of microfluidic formulation (SCALAR 1×, SCALAR 10×, PDMS 1×), while bulk mixed LNPs were significantly lower in potency (Fig. 4*G*). Similarly, we tested these luciferase mRNA LNPs in primary T cells (1:1 ratio of CD4+:CD8+) as a model cell type that is hard to transfect and found comparable potency between microfluidic-generated LNPs with minimal toxicity (*SI Appendix*, Fig. S13). Thus, we demonstrated that our SCALAR platform could produce mRNA LNPs at two different scales (1×, 10×) that were comparable to current PDMS small-scale microfluidic chips with respect to LNP physical properties and potency.

To demonstrate potent in vivo mRNA delivery using LNPs generated by our SCALAR chips, we formulated luciferase-encoding mRNA LNPs and compared potency of functional mRNA delivery for three microfluidic formulation methods: SCALAR 1× chip, SCALAR 10× chip, and PDMS 1× chip. We injected C57BL/6 mice intramuscularly to the right hind limb at 5 μg per mouse; 6 h later, we quantified the luminescent signal in major organs (heart, lungs, liver, spleen, and kidneys) and inguinal lymph nodes (Fig. 5 *A* and *B*). LNPs mainly transfected the injection sites and inguinal lymph nodes (iLN), with some transfection in the liver (Fig. 5*B*). We determined that there were no significant differences in mRNA delivery to the proximal inguinal lymph node between the formulation groups (Fig. 5*C*), although there is some variability due to dissection efficiency and luminescent measurements. Additionally, we found that there were no significant differences between the whole-body luminescent signal from the SCALAR 1×, SCALAR 10×, and PDMS 1× formulation groups (Fig. 5*D*). Thus, we demonstrated that our SCALAR platform can formulate mRNA LNPs for potent in vivo mRNA delivery with no differences between the scale of chip (1× or 10×) and similar potency to the PDMS small-scale microfluidic chip.

SARS-CoV-2 mRNA LNP Vaccine Production. To demonstrate the rapid production of vaccines using our SCALAR platform, we formulated mRNA LNPs for a vaccination study. Here, we vaccinated mice with a prime-and-boost strategy with a widely used vaccination route of intramuscular injection. The mRNA incorporated N1-methylpseudouridine (m1ψ) nucleoside modifications to avoid immune recognition and to improve translation. The m1ψ-modified SARS-CoV-2 mRNA encoded for the diproline modified Spike glycoprotein, where the mRNA coding sequence was identical to the mRNAs used in the two FDA-approved

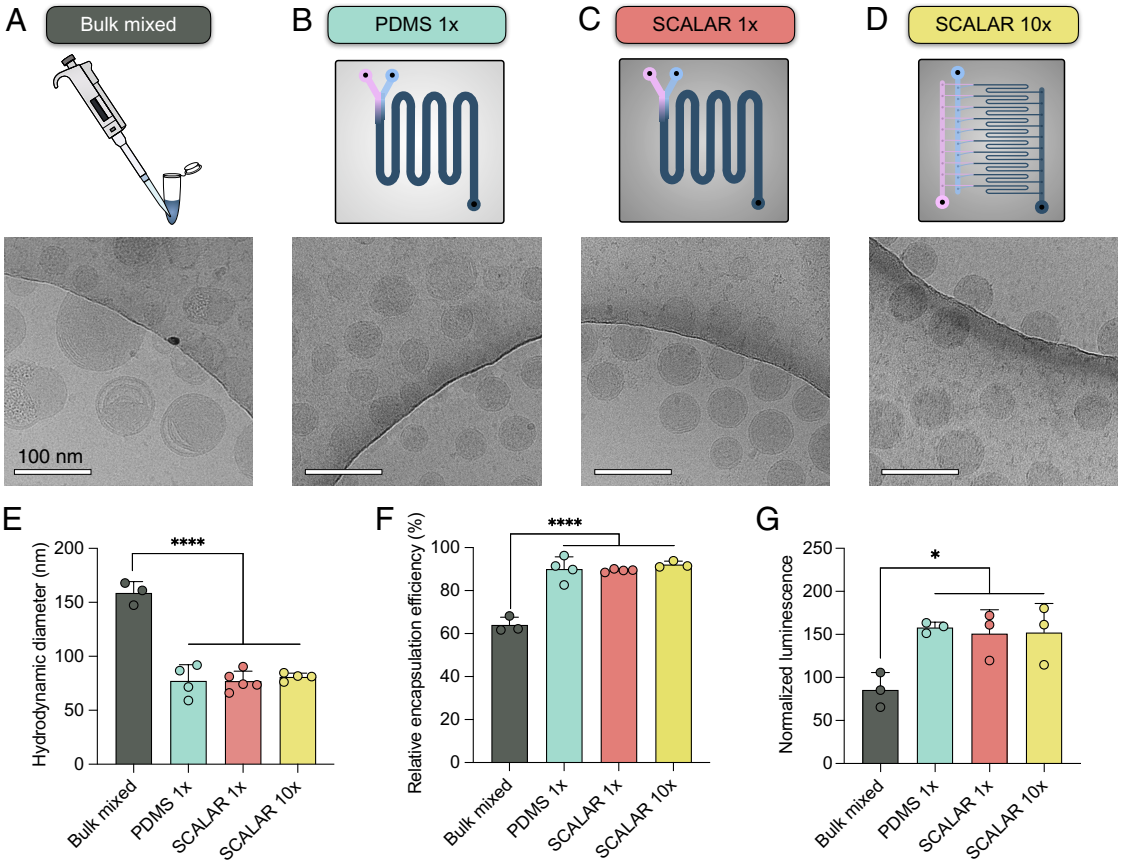

Fig. 4. Luciferase mRNA LNPs generated by SCALAR chips have similar physical properties and potency in vitro compared to standard PDMS microfluidic chips. (*A*) Cryo-TEM of luciferase mRNA LNPs produced by bulk mixing at 105 kx magnification. (Scale bar, 100 nm.) (*B*) Cryo-TEM of luciferase mRNA LNPs produced by the PDMS 1× chip at 105 kx magnification. (Scale bar, 100 nm.) (*C*) Cryo-TEM of luciferase mRNA LNPs produced by the SCALAR 1× chip at 105 kx magnification. (Scale bar, 100 nm.) (*D*) Cryo-TEM of luciferase mRNA LNPs produced by the SCALAR 10× chip at 105 kx magnification. (Scale bar, 100 nm.) (*E*) LNP diameter (±SD), quantified by intensity-based dynamic light scattering. ****$P < 0.0001$ in Tukey's multiple comparisons test between bulk mixing and microfluidic formulations. n = 3 to 5 independent LNP batches. (*F*) Relative mRNA encapsulation efficiency (±SD), quantified by a RiboGreen assay. ****$P < 0.0001$ in Tukey's multiple comparisons test between bulk mixing and microfluidic formulations. n = 3 to 5 independent LNP batches. (*G*) Luciferase expression of HepG2 cells treated with luciferase mRNA LNPs at 50 ng per 5,000 cells for 24 h. *$P < 0.05$ in Tukey's multiple comparisons test compared to bulk mixed LNPs. n = 3 biological replicates.

mRNA vaccines, Spikevax and Comirnaty (50). We formulated LNPs using the lipids mentioned previously (MC3, DSPC, cholesterol, DMG-PEG) and SARS-CoV-2 Spike-encoding mRNA using three microfluidic formulation methods: SCALAR 1×, SCALAR 10×, and PDMS 1×. Physical characterization (cryo-TEM morphology, size, encapsulation, pK_a, zeta potential) of LNPs indicated no significant differences between any of the microfluidic formulation techniques (*SI Appendix*, Fig. S14). We delivered the LNPs intramuscularly to C57BL/6 mice at days 0 and 14, respectively (Fig. 5*E*). On day 35, serum was collected and analyzed for the production of specific antibodies against the S1 subunit of the Spike protein using an endpoint dilution ELISA (Fig. 5*F*). The IgG titers reflect the vaccine efficacy and antibody responses, with comparable levels (10^6 to 10^7) to previous studies of SARS-CoV-2 vaccination (50, 51). We determined that our mRNA-LNPs induced high levels of S1-specific IgG; moreover, vaccine potency was comparable between all formulation methods with no significant differences in S1-specific antibody levels with mean titers 10^6 to 10^8. Altogether, these results suggest that our SCALAR platform can rapidly formulate mRNA LNPs at various scales for vaccine applications.

Formulation of LNPs at 17 L/h. To demonstrate the potential of this approach for industrial-scale manufacturing of LNPs, we generated sub-100-nm empty LNPs at a production rate of 17 L/h (Fig. 6 *E*–*G* and Movie S1). Our LNP formulation used C12-200, another gold-standard ionizable lipid (52), with lipids 1,2-dioleoyl-sn-glycero-3-phosphoethanolamine (DOPE) (53), cholesterol, and DMG-PEG. We used this formulation since we could synthesize C12-200 lipid at large scales (>1 g yield) (*SI Appendix*, Figs. S15–S17) at reasonable costs for these high-throughput experiments. Our custom-built pressure-driven flow system used pressure vessels to house the RNA aqueous input and lipid ethanol input (Fig. 6 *A* and *B* and Movie S1) and operate the chip at 100 PSI and 60 PSI for each input, respectively, to achieve a flow rate ratio of 3:1 at a total flow rate of 17 L/h. Our combination of ladder design geometry and branching architecture (Fig. 6 *C* and *D*) allowed us to reduce the operating pressure by 40% (100 PSI vs. 166 PSI) compared to a ladder design geometry alone (Fig. 6*E*). Cryo-TEM imaging confirmed that LNPs generated by the 256× SCALAR chip were comparable in morphology to LNPs generated by a SCALAR 1× and 10× chips (*SI Appendix*, Figs. S18 and S19). Additionally, we confirmed that LNP hydrodynamic diameter and concentration were comparable among all scales of silicon chips (1×, 10×, 256×) with a mean size of ~70 nm (Fig. 6*G*). We formulated empty LNPs for 27 min with our SCALAR 256× chip, demonstrating uniform size and LNP concentration among all fractions collected (Fig. 6*H*). Further, we demonstrated the formulation of RNA LNPs with our SCALAR 256× chip using polyA LNPs. PolyA was chosen as a substitute for mRNA as an economical approach for this study due to the

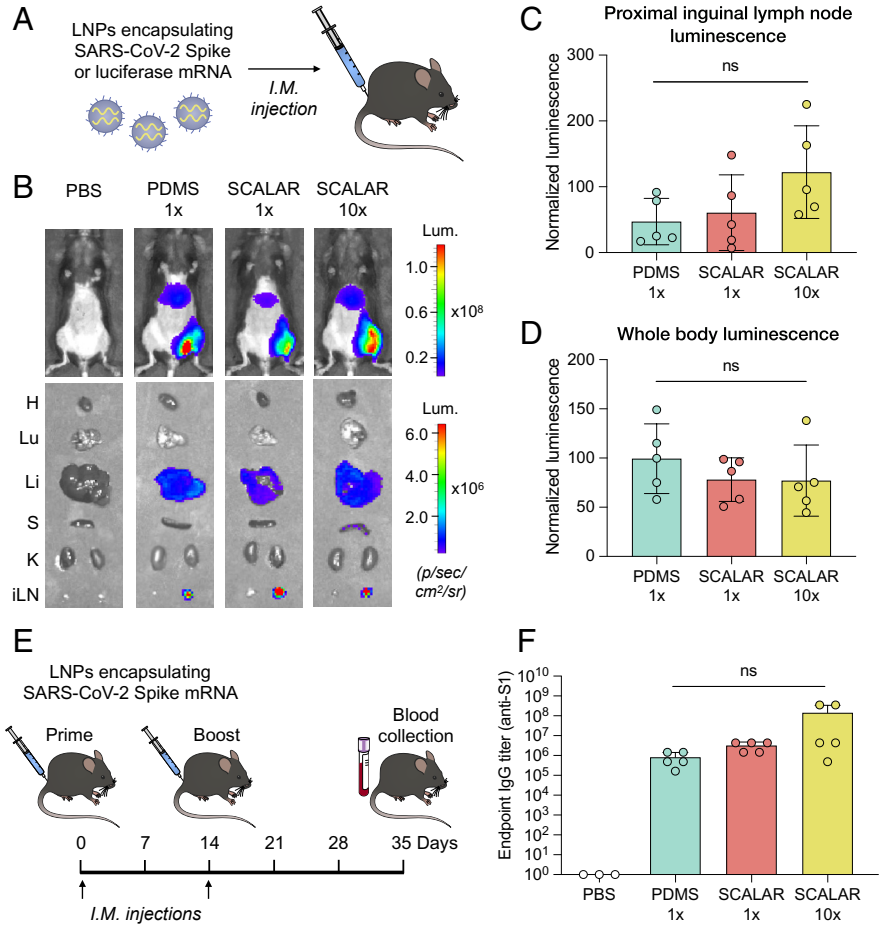

Fig. 5. SCALAR platform formulates potent mRNA LNPs for in vivo SARS-CoV-2 vaccination. (*A*) Luciferase mRNA LNPs were formulated by PDMS 1× chip, SCALAR 1× chip, or SCALAR 10× chip and administered to C57BL/6 mice via intramuscular injection at 5 μg per mouse. (*B*) Representative IVIS imaging at 6 h after LNP administration, showing luciferase expression in the proximal inguinal lymph node. H, heart; Lu, lungs; Li, liver; S, spleen; K, kidneys; iLN, inguinal lymph nodes. (*C*) Quantification of the luminescent signal (±SD) in the proximal inguinal lymph node. ns: $P = 0.1211$ in one-way ANOVA. n = 5 mice per formulation group. (*D*) Quantification of luciferase signal (±SD) in the whole body. ns: $P = 0.4810$ in one-way ANOVA. n = 5 mice per group. (*E*) Scheme of the prime and boost vaccination strategy using SARS-CoV-2 Spike-encoding mRNA LNPs. C57BL/6 mice were immunized twice with 1 μg Spike mRNA LNPs at days 0 and 14, and serum was collected on day 35. (*F*) S1-specific IgG titer (±SD) was determined by endpoint dilution ELISA. ns: $P = 0.1070$ in one-way ANOVA between LNP formulation groups. n = 3 mice for PBS group; n = 5 mice per LNP formulation group.

cost and complexity of obtaining mRNA at this scale. PolyA LNPs generated by the SCALAR 1×, 10×, or 256× chips were comparable with respect to relative encapsulation efficiency, zeta potential (Fig. 6*I*), size, and LNP concentration (Fig. 6*J*). Additionally, we demonstrated that our 256× chip could formulate polyA LNPs for 23 min with no significant differences in LNP size or concentration (Fig. 6*K*). Thus, we have validated the use of our SCALAR platform at any scale (1×, 10×, or 256×) for high-throughput production of RNA LNPs with controlled physical properties.

Discussion

Here, we have developed a SCALAR platform to mass produce RNA LNPs for vaccine and therapeutic applications in a manner that can be compatible with pharmaceutical manufacturing. These chips are fabricated entirely out of silicon and glass substrates, which have excellent solvent compatibility, are compatible with high-temperature sterilization, and can be fully reset and reused. Our approach directly addresses the disconnect between formulation techniques at the small-scale discovery stage and formulation techniques at the large scale used for clinical testing and translation. Further, our throughput-invariant system uses the same staggered herringbone micromixer design with the same dimensions at the 1×, 10×, or 256× scale, thus eliminating the concern for variability or minute differences in LNP physical properties or potency during scale-up. Throughout this study, we have validated the design of the SCALAR chips, formulated SARS-CoV-2 Spike mRNA LNPs for vaccination in mice, and demonstrated robust RNA LNP formulation at 17 L/h for >20 min.

While other studies have formulated LNPs at high production rates (>5 L/h) using the NanoAssemblr platform or T-junction mixing, many of these techniques cannot scale past 10× since the complexity of fluid handling requires individual sets of inputs and outputs for each chip. Alternatively, our platform can easily scale to >1,000× and could be feasible for use in the pharmaceutical industry. If produced at scale, one 256× chip could be fabricated for approximately $100 (41). Further, since these chips are fabricated using anodically bonded silicon and glass, it can operate at significantly higher pressures (>1,000 PSI) than typical PDMS devices, making it particularly well suited for high-throughput processing of highly viscous fluids. While we chose to fabricate these chips using 4-inch silicon wafers, one could use 6-inch or 12-inch wafers (41) to incorporate >1,000 mixing units onto a single chip. Further, since the flow resistors decouple the design of the mixing unit and the fluidics required for parallelization, these mixing units can be modified to accommodate any desired architecture, such as bifurcating mixers, baffle mixers, or mixers designed for particular applications. Additionally, due to the complexity of cold chain storage conditions for mRNA therapeutics and vaccines that limit access to vaccines in resource-poor countries, (54) these chips could be used for point-of-demand pharmaceutical production at locations convenient to the patient.

One limitation of this work is the fouling of microchannels during RNA LNP formulations. This phenomenon has been well documented for microfluidic systems, and there are a few strategies to overcome this challenge. The chip could be monitored with flow meters (55) during operation to ensure that the total flow rate remains constant, and then a cleaning solution could be used as needed or on a regular period to reset the chip (e.g., every 15 min, as shown in Fig. 3) and the LNP formulation could continue. This provides advantages compared to current microfluidic chips fabricated in cyclic olefin copolymer (COC), which have

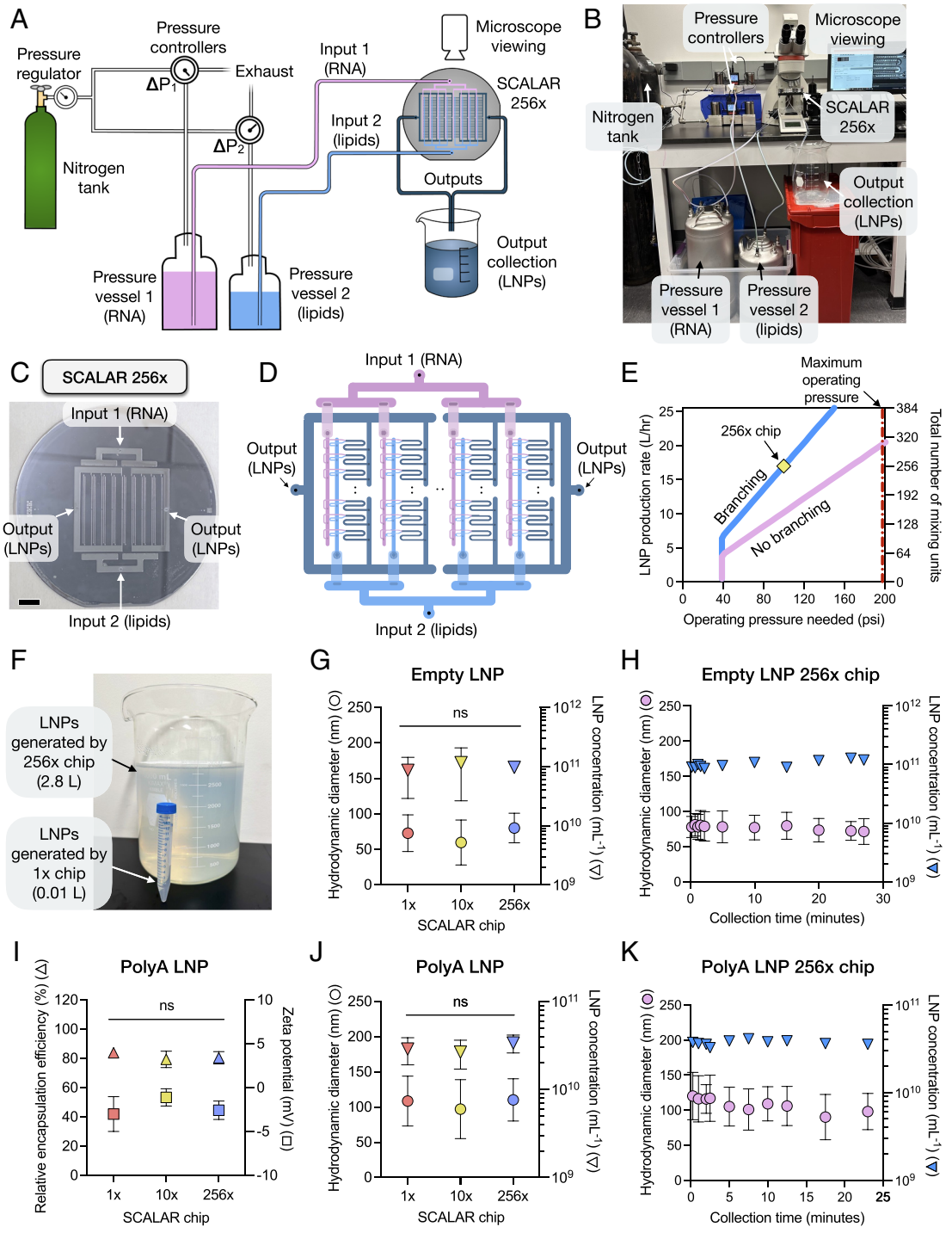

Fig. 6. High-throughput (17 L/h) production of LNPs at moderate pressures (100 PSI) using a SCALAR 256× chip. (*A* and *B*) Experimental setup to test the 256× chip by a custom pressure-driven flow system, showing the setup schematic (*A*) and an image of the setup (*B*). (*C*) Image of the 256× chip showing the inputs/outputs corresponding to the schematic in *D*. (*D*) Schematic of chip design summarizing the incorporation of branching geometry and ladder design architecture to uniformly distribute inputs to each mixing unit. Schematic is not to scale. (*E*) Advantages of the branching geometry to reduce the pressure needed to run a parallelized chip. Curves plotted are the theoretical operating pressure needed for chips that incorporate a certain number of mixing units (*Right y* axis), arranged in eight rows that are all in parallel ('no branching'; blue curve) or two sets of four rows that are connected by a branching unit ('branching'; pink curve). Our 256× chip is highlighted. The incorporation of branching (pink curve) reduced the necessary pressure by over 40% compared to an unbranched design (blue curve) for 256 total mixing units. The dashed red line indicates the maximum operating pressure for these chips using our experimental setup. (*F*) Image showing the relative throughput of 1× and 256× SCALAR chips that produced LNPs for 10 min with resultant volumes of 2.8 L (256× chip; shown in a 3.5-L beaker) or 0.01 L (1× chip; shown in a 15-mL conical tube). (*G* and *H*) Physical characterization of empty LNPs produced by a 256× SCALAR chip compared to 1× and 10× chips. (*G*) Size and LNP concentration measurements (±SD) indicated that there were no differences between LNPs produced by the SCALAR 1×, 10×, or 256× chips. Size and concentration data from n = 6 to 12 LNP samples (1×: n = 6; 10×: n = 12; 256×: n = 11) were combined and plotted. Samples were compared by a two-way ANOVA, ns: $P = 0.1714$. (*H*) Size and concentration (±SD) of empty LNPs produced by a SCALAR 256× chip over 27 min. n = 3 size measurements and n = 6 concentration measurements per sample. (*I*-*K*) Physical characterization of polyA LNPs produced by a SCALAR 256× chip compared to 1× and 10× chips. (*I*) Relative polyA encapsulation efficiency (±SD) and zeta potential (±SD) of polyA LNPs produced by SCALAR 1×, 10×, or 256× chips. Samples were compared by a two-way ANOVA, $P = 0.4182$. (*J*) Size and LNP concentration measurements (±SD) indicated that there were no differences between LNPs produced by the SCALAR 1×, 10×, or 256× chips. Samples were compared by a two way ANOVA, $P = 0.0717$. (*K*) Size and concentration (±SD) of empty LNPs produced by a SCALAR 256× chip over 23 min. n = 3 size measurements and n = 6 concentration measurements per sample.

limited reuse due to interactions of LNP formulation components and chip material (56). Another approach could implement coatings that would reduce interactions of RNA and lipid components with the channel walls to prevent adsorption of materials and eventual channel blockages. An advancement in antifouling coatings for LNP formulations would be essential to the field.

In summary, we have developed a SCALAR platform to produce RNA LNPs on the small-scale (0.1 L/h) and large-scale (17 L/h) without altering the desirable physical properties and potency typical of microfluidic-generated LNPs. These chips can address challenges in the formulation of LNPs for RNA therapeutics and vaccines and can be broadly applied to nanoparticle formulations that are based on rapid mixing of reagents.

Materials and Methods

Chip Fabrication. The chips were fabricated in the Quattrone Nanofabrication Facility at the University of Pennsylvania. The chip has four mask layers which were designed in AutoCAD (Autodesk, San Rafael, CA) to define the delivery channels (layer 1), mixing channels (layer 2), herringbones and resistors (layer 3), and through silicon vias (etching layer 4; layer 5 overall). The design of each layer was patterned onto chrome-coated soda lime photomasks (AZ1500; Telic Company, Santa Clarita, CA) using a Heidelberg 66 plus laser writer with a 10-mm write head. Photomasks were developed in the AZ 300MIF developer (EMD Performance Materials Corp., Philadelphia, PA) for 90 s and then in chromium etchant (Transene Company, Danvers, MA) for 2 min; the remaining photoresist was removed by Remover 1,165 (DuPont, Wilmington, DE) with sonication at 60 °C for 1 min. To fabricate the chip, each layer is lithographically patterned onto a single 100-mm silicon wafer (ID 775; University Wafer, South Boston, MA) followed by deep reactive ion etching (DRIE) to define the channels. For the lithography, S1805 photoresist (Dow, Midland, MI) is mixed with acetone (1:8), and the resist is spray-coated to the desired thickness using an AS8 AltaSpray Coater (SUSS MicroTec, Garching, Germany).

In the first etching layer, the wafer is dipped in 49% hydrofluoric acid (HF) to improve photoresist adhesion; then, 16 μm of photoresist is spray-coated onto the front side of the silicon wafer. The wafer is left idle at room temperature for 1 h for rehydration, soft baked at 110 °C for 8 min, and then left idle at room temperature for 45 min before exposure. All bakes are performed in an oven. The delivery channel design is exposed using an MA6 mask aligner (SUSS MicroTec); then, the wafer is baked at 110 °C for 2 min and left idle at room temperature for rehydration for 30 min. The wafer is developed in AZ 300MIF developer, rinsed with water, dried with N_2, and baked at 110 °C for 10 min. The wafer is etched using DRIE (SPTS Rapier Si DRIE, Newport, UK) to a 370-μm etch depth, cleaned using acetone and isopropanol for 5 min each, and then cleaned by immersion in Nano-Strip (CMC Materials, Aurora, IL) heated to 110 °C for an hour followed by cleaning in a Spin Rinse Dryer (SRD; RENA Compass, RENA, Albany, OR). For the second etching layer, the wafer is dipped in 49% HF; then, the backside of the wafer is coated with 8 μm of photoresist, left idle at room temperature for 20 min, baked at 110 °C for 4 min, and then exposed with the mixing channel design. The wafer is then left idle at room temperature for 20 min, developed, baked at 110 °C for 5 min, and then etched to a 70-μm etch depth using DRIE. The wafer is then cleaned using acetone, isopropanol, Nano-Strip, and SRD as before. For the third etching layer, the wafer is dipped in 49% HF; then, the backside of the wafer is coated with 4 μm of photoresist, left idle at room temperature for 20 min, baked at 110 °C for 2 min, and then exposed with the herringbone and resistor design. The wafer is then left idle at room temperature for 20 min, developed, baked at 110 °C for 4 min, etched to a 25-μm etch depth using DRIE, and then cleaned using acetone, isopropanol, Nano-Strip, and SRD as before. Using plasma-enhanced chemical vapor deposition (Oxford Plasma Lab 100 PECVD) (Oxford Instruments, Abingdon, UK), 4 μm of SiO_2 is deposited onto the backside of the wafer at a rate of 0.3 μm per min, and then the wafer is cleaned using Nano-Strip and SRD. The SiO_2 acts as an etch-stop layer for DRIE (43) to circumvent the need for temporary adhesives or carrier wafers when etching through silicon vias. For the fourth etching layer, the front side of the wafer is coated with 8 μm of photoresist, left idle at room temperature for 20 min, baked at 110 °C for 4 min, and then exposed with the through silicon via design. The wafer is left idle at room temperature for 20 min, developed, baked at 110 °C for 5 min, and then etched to a 60-μm etch depth using DRIE. The wafer is then cleaned using acetone and isopropanol as before, and then, the SiO_2 layer is removed by immersion in 25% HF for 5 min. The etched silicon wafer and a 100-mm Borofloat 33 glass wafer (ID 517; University Wafer) are cleaned using Nano-Strip and SRD as before. Another Borofloat 33 glass wafer is micromachined with 1-mm holes that serve as inlets and outlets for the chip using an IX-255 laser system (IPG Photonics, Oxford, MA); then, this wafer is cleaned using Nano-Strip and SRD as before. Finally, the three wafers (glass/silicon/glass) are stacked together and anodically bonded on each side using an EVG 510 Wafer Bonding System (EVG Group, Oberosterreich, Austria) at 900 v with a 1,000-N piston force at 400 °C (*SI Appendix*, Fig. S3).

Experimental Setup. To connect the silicon and glass chip to a fluidic handling system, a custom housing system was designed in SOLIDWORKS (Dassault Systèmes, Vélizy-Villacoublay, France) and machined out of Aluminum 6061-T651 (Protolabs, Maple Plain, MN) with 1/4″ – 28 UNF threaded connections on the front side of the chip for the inputs/outputs and an observation window on the backside of the chip to observe the mixing channels (*SI Appendix*, Figs. S4 and S5). Aluminum pieces were 6.35-mm thick each for 1× and 10× chip holders; pieces were 8 mm thick each for 256× chip holders. An acrylic centering piece was laser cut to align the chip in the housing system for 1× and 10× chips (*SI Appendix*, Fig. S4), where the acrylic piece was thinner than the wafer stack such that the aluminum makes contact directly with the silicon or glass surfaces of the chip. Bonded wafer stacks are either 1 mm thick (1×) or 1.5 mm thick (10×, 256× chips). Of note, 256× chips were manually aligned between the aluminum plates since there was variation (± 2 mm) in the bonded chip (glass–silicon–glass stack) diameter. A custom-built pressure-driven flow system (Fig. 6 *A* and *B*) rated to 200 PSI delivered fluids to the chip. A nitrogen tank was connected to two dual-valve pressure controllers (Alicat Scientific, Tucson, AZ) that controlled the RNA and lipid inputs using FlowVision 2.0 software (Alicat Scientific). The pressure controllers were connected to 5-gallon and 3-gallon T-304 stainless steel pressure vessels (Alloy Products Corp., Waukesha, WI), where the 5-gallon vessel was used for the RNA input and the 3-gallon vessel was used for the lipid input. Connections between the nitrogen tank, pressure controllers, and pressure vessels used PTFE tubing with a 1/4″ OD (Part 52365K61; McMaster-Carr, Elmhurst, IL) and 316 stainless steel compression fittings (Parts 52245K521, 52245K533; McMaster-Carr). Pressure vessels were connected to the chip using 1/4″ OD PTFE tubing and 1/8″ OD FEP tubing (Part 52355K41; McMaster-Carr) that were connected with 316 stainless steel compression fittings (Part 8239K232; McMaster-Carr). ETFE flangeless fittings (Part XP-348, Idex Corporation, Lake Forest, IL) connected the 1/8″ OD tubing to the aluminum housing system. The housing system was mounted on an xyz translational stage (*SI Appendix*, Fig. S4) to monitor individual device performance during operation.

Mixing Characterization. Mixing efficiency of the chips was evaluated as previously described (57). Briefly, 10 kDa FITC-dextran (Item FD10S; MilliporeSigma, Burlington, MA) and 10 kDa rhodamine B isothiocyanate-dextran (Item R8881; MilliporeSigma) were dissolved to 20 μM in water, filtered with a 0.22-μm PES filter, and flowed through chips at a total flow rate of 0.072 L/h (1× chip), 0.72 L/h (10× chip), or 20 L/h (256× chip). Fluorescence images of the channel were taken at different channel lengths, and the intensity profile of each dye across the channel was quantified using ImageJ (NIH) for numerical analysis in MATLAB (MathWorks, Natick, MA). The background was subtracted from the dye intensity profiles; then, the profiles were normalized to the maximum intensity, and a mixing value was calculated by quantifying the area under the curve for the difference of the rhodamine B normalized intensity from the FITC normalized intensity. This mixing value ranged from 1 (solutions not mixed) to 0 (solutions completely mixed), where a value of 0.1 was used to indicate 90% mixing. An exponential decay model was used to calculate the SE.

Lipid Synthesis. The ionizable lipid C12-200 (1,1′-((2-(4-(2-((2-(bis(2-hydroxydodecyl)amino)ethyl)(2-hydroxydodecyl)amino)ethyl)piperazin-1-yl)ethyl)azanediyl)bis(dodecan-2-ol)) was synthesized by adding N^1-(2-(4-(2-aminoethyl)piperazin-1-yl)ethyl)ethane-1,2-diamine (1.00 g, 4.64 mmol, 1.0 equiv.), ethanol (10 mL), and 1,2-epoxydodecane (7.10 mL, 32.5 mmol, 7.0 equiv.) to a 50-mL round-bottom flask with a stir bar. The reaction was stirred at 80 °C for 48 h.

Afterward, the ethanol was removed in vacuo and then diluted in 15 mL dichloromethane (DCM). The compound was purified using a CombiFlash (Teledyne ISCO, Lincoln, NE) using a 40 g RediSep Gold® silica gel flash column using a gradient mobile phase from 100% DCM to 20% DCM and 80% Ultra solution (75% DCM, 22% methanol, and 3% ammonium hydroxide) over 30 min. The solution was run purified in two runs, using half of the DCM mixture each time. C12-200 was isolated as a yellow-orange oil in 37% yield and characterized by ^{1}H NMR, ^{13}C NMR, and LC-MS (*SI Appendix*, Figs. S12–S14).

^{1}H NMR and ^{13}C NMR spectra were obtained on a NEO 400 MHz spectrometer using d-chloroform as the solvent. LC-MS was performed on an Agilent LCMS system equipped with UV–Vis and evaporative light scattering detectors (ELSD). Flash chromatography was performed on a Teledyne ISCO CombiFlash Rf-200i chromatography system equipped with UV-Vis and ELSD.

LNP Formulation and Characterization. LNPs were formulated using a microfluidic chip or pipette mixing by rapid mixing of an aqueous phase containing RNA with an ethanol phase containing lipid components. The aqueous phase consisted of mRNA or polyA (Roche, Product 10108626001) diluted to 74 μg/mL in 10 mM citrate buffer (Alpha Teknova, Inc., Hollister, CA). mRNA encoding for mCherry or GFP was purchased from TriLink (L-7201, L-7203; TriLink BioTechnologies, San Diego, CA); mRNA encoding for firefly luciferase or Spike was gifted from the Weissman lab. The ethanol phase contained D-Lin-MC3-DMA (HY-112251; MedChemExpress, Monmouth Junction, NJ), 1,2-distearoyl-sn-glycero-3-phosphocholine (DSPC, Product 850365; Avanti Polar Lipids, Alabaster, AL), cholesterol (Sigma-Aldrich, St. Louis, MO), and DMG-PEG 2000 (Product 880151; Avanti Polar Lipids) in ethanol at molar ratios of 50%, 10%, 38.5%, and 1.5%, respectively. The ionizable lipid to mRNA weight ratio was 10:1 for all formulations. LNPs formulated by the 10× or 256× chip had reagents diluted by 3× to preserve reagents. For the large-scale LNP formulation in the 256× chip, LNPs were formulated with the synthesized ionizable lipid C12-200, phospholipid 1,2-dioleoyl-sn-glycero-3-phosphoethanolamine (DOPE, Product 850725; Avanti Polar Lipids), cholesterol, and DMG-PEG 2000 at molar ratios of 50%, 10%, 38.5%, and 1.5%, respectively.

Using the custom pressure-driven flow system, the aqueous phase with RNA and the ethanol phase with lipids were infused at a flow rate ratio of 3:1 with a total volumetric flow rate per mixing channel of 1.1 to 1.2 mL/min. LNPs were dialyzed against 1× PBS in 20-kDa MWCO dialysis cassettes (Products 87734, 87735; Thermo Fisher, Waltham, MA) for 2 h before filtration by 0.22-μm PES filters (Product 25-243; Genesee Scientific, Morrisville, NC). LNPs were stored at 4 °C for future use. If needed, LNPs were concentrated using 50- or 100-kDa MWCO centrifugal filters (Product UFC205024, UFC210024; MilliporeSigma). For pipette-mixed LNPs, an Eppendorf Xplorer Electronic Pipette (Thermo Fisher) set to the pipette/mixing mode mixed the reagents at the maximum speed for 50 cycles; after dialysis, LNPs were filtered using a 0.45-μm PES filter (Product 25 to 245, Genesee Scientific). For chip reuse experiments, chips were flushed with 1% triton X for 5 min, nitrogen for 1 min, and then ethanol for 5 min between formulations. For chip autoclaving, the SCALAR chip was disassembled from the tubing and device holder; then, the chip was placed into a glass beaker, and a standard glass sterilization cycle was performed.

To characterize the LNPs, LNPs were diluted 1:30 in 1× PBS and a combination of dynamic and static light scattering was performed using a DynaPro Plate Reader III (Wyatt Technology, Santa Barbara, CA) to quantify hydrodynamic size, polydispersity index (PDI), and LNP concentration. Sizes reported are intensity-weighted averages, and SD of LNP size is calculated by $\sigma = (\text{PDI} * \text{diameter}^2)^{1/2}$. RNA concentration was measured by 260-nm absorbance using a Tecan NanoQuant Plate (Thermo Fisher) and an Infinite M Plex plate reader (Tecan, Männedorf, Switzerland). Relative encapsulation efficiency was measured using a RiboGreen Quant-it RNA assay kit (Thermo Fisher) per the manufacturer instructions and reported as a percentage of encapsulated RNA to total RNA in the sample. For zeta potential measurements, LNPs were diluted 1:100 in DI water and measured using a Zetasizer Nano (Malvern Instruments, Malvern, UK). To quantify pK_a, a 6-(p-toluidinyl) naphthalene-2-sulfonic acid (TNS) assay was performed as previously described (58). For the cryo-TEM imaging, 3 μL of LNPs at a concentration of ~100 ng per μL mRNA were applied to a Quantifoil holey carbon grid which had been glow discharged. Grids were blotted and plunge frozen in liquid ethane using a Vitrobot Mark IV (Thermo Scientific). Imaging was performed at the Beckman Center for cryo-EM on a Titan Krios (Thermo Scientific) equipped with a K3 Bioquantum at 64 kx or 105 kx magnification. ImageJ was used to measure LNP sizes from the cryo-TEM images.

mRNA Delivery In Vitro and Ex Vivo. Jurkat cells (TIB-152, ATCC) were cultured in RPMI-1,640 with L-glutamine (Thermo Fisher) supplemented with 10% fetal bovine serum and 1% penicillin–streptomycin; HepG2 cells were cultured in DMEM supplemented with 10% fetal bovine serum and 1% penicillin–streptomycin. Jurkats were plated at 60k cells per 60 μL in a 96-well plate and treated with luciferase mRNA LNPs, mCherry mRNA LNPs or GFP mRNA LNPs. HepG2 cells were plated at 5k cells per 100 μL in a 96-well plate and treated with luciferase mRNA LNPs 24 h after plating. Luminescence was measured 24 h after LNP treatment using a Luciferase Assay System (E4550; Promega, Madison, WI) per the manufacturer's protocol. Luminescent measurements were normalized to untreated cells on the same plate. mCherry and GFP expression was measured at 24 h using flow cytometry.

Primary human CD4+ and CD8+ T cells were obtained from the Human Immunology Core at the University of Pennsylvania. Cells were activated overnight with Human T-activator CD3/CD28 Dynabeads (Thermo Fisher) at a 1:1 cell:bead ratio in supplemented RPMI medium. CD4+ and CD8+ T cells were counted and combined at a 1:1 ratio, plated at 60k cells per well in a 96-well plate and treated with luciferase mRNA LNPs; luminescence was measured 24 h later with a Tecan Infinite M Plex plate reader using a Luciferase Assay System. Luminescent measurements were normalized to untreated cells on the same plate. Cell viability was measured by a CellTiter-Glo assay (G7572; Promega) per the manufacturer's protocol and normalized to untreated cells.

Animal Studies. All animal procedures were performed on female C56BL/6 mice aged 6 to 8 wk (The Jackson Laboratory) in accordance with protocols approved by the Institutional Animal Care and Use Committee (IACUC) of the University of Pennsylvania. For the luciferase study, mice were injected by intramuscular injection with luciferase mRNA LNPs at an mRNA dose of 5 μg per mouse. At 6 h postinjection, mice were intraperitoneally injected with D-luciferin potassium salt at 150 mg/kg. Bioluminescence imaging of the whole body and dissected major organs as well as inguinal lymph nodes was performed on an in vivo imaging system (IVIS; PerkinElmer, Waltham, MA). Bioluminescence values were quantified by measuring photon flux in the region of interest using Living Image 4.7.3 software (PerkinElmer), and photon flux values were normalized to the background of each image.

For the immunization study, mice were intramuscularly injected with SARS-CoV-2 mRNA LNPs at a dose of 1 μg mRNA per mouse twice using a prime and boost strategy at a 2-wk interval. At week five (day 35), blood was collected through the retro-orbital route and transferred into serum separator tubes (SKU 365967; BD, Franklin Lakes, NJ). Serum was incubated at room temperature for 30 min, centrifuged at 10,000 g for 5 min, and then collected and stored at −20 °C.

To quantify anti-S1 antibody titers using ELISA, High Bind Stripwell Corning 96-Well Clear Polystyrene Microplates were coated overnight with 1 μg/mL purified SARS-CoV-2 His–tagged S1. Plates were washed once with wash buffer (0.05% Tween-20 in PBS) and blocked for 2 h at room temperature using a solution of heat-inactivated, IgG-depleted, protease-free bovine serum albumin (2% w/v BSA in PBS). After blocking, plates were washed three times, and mouse sera were serially diluted in the blocking solution and incubated for 2 h at room temperature. Plates were washed three times before the addition of HRP-conjugated anti-mouse secondary antibody specific to total IgG (1:10,000) in blocking buffer. Plates were incubated for 1.5 h, washed three times before the addition of 100 μL per well of KPL TMB substrate for 8 min. The reaction was stopped by adding 50 μL of 2N sulfuric acid, and the absorbance was measured at 450 nm using a SpectraMax 190 microplate reader. S1-specific IgG end point dilution titer was defined as the highest dilution of serum to give an OD greater than the cutoff OD value determined using the Frey method (59).

Statistical Information. Statistical tests were performed by GraphPad Prism 9. Data are presented as mean ± SD unless otherwise specified. Student's *t*-test or one-way (ANOVA) followed by Tukey's multiple comparisons test was used to compare between two groups or several groups, respectively. $P < 0.05$ was considered statistically significant.

Data, Materials, and Software Availability. All study data are included in the article and/or supporting information.

ACKNOWLEDGMENTS. This work was carried out in part at the Singh Center for Nanotechnology, which is supported by the NSF National Nanotechnology Coordinated Infrastructure Program under grant NNCI-2025608. Cryo-EM imaging was provided by the Beckman Center for Cryo Electron Microscopy at the University of Pennsylvania Perelman School of Medicine (RRID: SCR_022375). M.J.M. acknowledges support from a US (NIH) Director's New Innovator Award (DP2 TR002776), a Burroughs Wellcome Fund Career Award at the Scientific Interface (CASI), and the NIH (NCI R01 CA241661, NCI R37 CA244911, and NIDDK R01 DK123049). This work was partially supported by the Wellcome Leap R3 program. D.I. acknowledges support from the National Cancer Institute (5R21CA236653 and 5RM1HG010023) and NIH (R01HL160616). S.J.S. is supported by an NSF Graduate Research Fellowship (Award 1845298). M.S.P. acknowledges support from the National Institute of Dental and Craniofacial Research of the NIH (T90DE030854). The content is solely the responsibility of the authors and does not necessarily represent the official views of the NIH.

Author affiliations: [a]Department of Bioengineering, University of Pennsylvania, Philadelphia, PA 19104; [b]Department of Chemical and Biomolecular Engineering, University of Pennsylvania, Philadelphia, PA 19104; [c]Department of Medicine, University of Pennsylvania, Philadelphia, PA 19104; [d]Department of Biochemistry and Biophysics, Perelman School of Medicine, University of Pennsylvania, Philadelphia, PA 19104; [e]Department of Electrical and Systems Engineering, University of Pennsylvania, Philadelphia, PA 19104; [f]Institute for Immunology, Perelman School of Medicine, University of Pennsylvania, Philadelphia, PA 19104; [g]Cardiovascular Institute, Perelman School of Medicine, University of Pennsylvania, Philadelphia, PA 19104; [h]Institute for Regenerative Medicine, Perelman School of Medicine, University of Pennsylvania, Philadelphia, PA 19104; [i]Abramson Cancer Center, Perelman School of Medicine, University of Pennsylvania, Philadelphia, PA 19104; and [j]Penn Institute for RNA Innovation, Perelman School of Medicine, University of Pennsylvania, Philadelphia, PA 19104

1. N. Pardi, M. J. Hogan, F. W. Porter, D. Weissman, mRNA vaccines-a new era in vaccinology. *Nat. Rev. Drug Discov.* **17**, 261–279 (2018).
2. N. Pardi, M. J. Hogan, D. Weissman, Recent advances in mRNA vaccine technology. *Curr. Opin. Immunol.* **65**, 14–20 (2020).
3. T. Schlake, A. Thess, M. Fotin-Mleczek, K. J. Kallen, Developing mRNA-vaccine technologies. *RNA Biol.* **9**, 1319–1330 (2012).
4. X. Han *et al.*, An ionizable lipid toolbox for RNA delivery. *Nat. Commun.* **12**, 8–13 (2021).
5. R. Zhang *et al.*, Helper lipid structure influences protein adsorption and delivery of lipid nanoparticles to spleen and liver. *Biomater. Sci.* **9**, 1449–1463 (2021), 10.1039/d0bm01609h.
6. K. T. Love *et al.*, Lipid-like materials for low-dose, in vivo gene silencing. *Proc. Natl. Acad. Sci. U.S.A.* **107**, 1864–1869 (2010).
7. J. A. Kulkarni *et al.*, On the formation and morphology of lipid nanoparticles containing ionizable cationic lipids and siRNA. *ACS Nano* **12**, 4787–4795 (2018).
8. X. Hou, T. Zaks, R. Langer, Y. Dong, Lipid nanoparticles for mRNA delivery. *Nat. Rev. Mater.* **6**, 1078–1094 (2021).
9. Y. Y. C. Tam, S. Chen, P. R. Cullis, Advances in lipid nanoparticles for siRNA delivery. *Pharmaceutics* **5**, 498–507 (2013).
10. E. Kon, U. Elia, D. Peer, Principles for designing an optimal mRNA lipid nanoparticle vaccine. *Curr. Opin. Biotechnol.* **73**, 329–336 (2022).
11. A. C. Anselmo, S. Mitragotri, Nanoparticles in the clinic: An update. *Bioeng. Transl. Med.* **4**, 1–16 (2019).
12. R. L. Ball, K. A. Hajj, J. Vizelman, P. Bajaj, K. A. Whitehead, Lipid nanoparticle formulations for enhanced co-delivery of siRNA and mRNA. *Nano Lett.* **18**, 3814–3822 (2018).
13. Q. Cheng *et al.*, Selective organ targeting (SORT) nanoparticles for tissue-specific mRNA delivery and CRISPR-Cas gene editing. *Nat. Nanotechnol.* **15**, 313–320 (2020), 10.1038/s41565-020-0669-6.
14. A. K. Blakney *et al.*, The skin you are in: Design-of-experiments optimization of lipid nanoparticle self-amplifying RNA formulations in human skin explants. *ACS Nano* **13**, 5920–5930 (2019).
15. E. Cott, E. DeBruyn, C. Corum, *How Pfizer Makes Its Covid-19 Vaccine* (New York Times, 2021).
16. M. J. W. Evers *et al.*, State-of-the-art design and rapid-mixing production techniques of lipid nanoparticles for nucleic acid delivery. *Small Methods* **2**, 1700375 (2018).
17. S. J. Shepherd, D. Issadore, M. J. Mitchell, Microfluidic formulation of nanoparticles for biomedical applications. *Biomaterials* **274**, 120826 (2021).
18. X. Wang *et al.*, Preparation of selective organ-targeting (SORT) lipid nanoparticles (LNPs) using multiple technical methods for tissue-specific mRNA delivery. *Nat. Protoc.* **18**, 265–291 (2023).
19. L. Corey, J. R. Mascola, A. S. Fauci, F. S. Collins, A strategic approach to COVID-19 vaccine R&D. *Sci. Policy Forum* **368**, 948–950 (2020).
20. T. Le Thanh *et al.*, The COVID-19 vaccine development landscape. *Nat. Rev. Drug Discov.* **19**, 305–306 (2020).
21. S. S. Rosa, D. M. F. Prazeres, A. M. Azevedo, M. P. C. Marques, mRNA vaccines manufacturing: Challenges and bottlenecks. *Vaccine* **39**, 2190–2200 (2021).
22. Z. Kis, C. Kontoravdi, R. Shattock, N. Shah, Resources, production scales and time required for producing RNA vaccines for the global pandemic demand. *Vaccines* **9**, 1–14 (2021).
23. N. M. Belliveau *et al.*, Microfluidic synthesis of highly potent limit-size lipid nanoparticles for in vivo delivery of siRNA. *Mol. Ther. Nucleic Acids* **1**, e37 (2012).
24. D. Chen *et al.*, Rapid discovery of potent siRNA-containing lipid nanoparticles enabled by controlled microfluidic formulation. *J. Am. Chem. Soc.* **134**, 6948–6951 (2012).
25. C. B. Roces *et al.*, Manufacturing considerations for the development of lipid nanoparticles using microfluidics. *Pharmaceutics* **12**, 1–19 (2020).
26. R. R. Hood, D. L. Devoe, J. Atencia, W. N. Vreeland, D. M. Omiatek, A facile route to the synthesis of monodisperse nanoscale liposomes using 3D microfluidic hydrodynamic focusing in a concentric capillary array. *Lab Chip* **14**, 2403–2409 (2014).
27. A. Jahn *et al.*, Microfluidic mixing and the formation of nanoscale lipid vesicles. *ACS Nano* **4**, 2077–2087 (2010).
28. C. Webb *et al.*, Using microfluidics for scalable manufacturing of nanomedicines from bench to GMP: A case study using protein-loaded liposomes. *Int. J. Pharm.* **582**, 119266 (2020).
29. N. Kimura *et al.*, Development of the iLiNP device: Fine tuning the lipid nanoparticle size within 10 nm for drug delivery. *ACS Omega* **3**, 5044–5051 (2018).
30. A. K. K. Leung, Y. Y. C. Tam, S. Chen, I. M. Hafez, P. R. Cullis, Microfluidic mixing: A general method for encapsulating macromolecules in lipid nanoparticle systems. *J. Phys. Chem. B* **119**, 8698–8706 (2015).
31. J. M. Lim *et al.*, Parallel microfluidic synthesis of size-tunable polymeric nanoparticles using 3D flow focusing towards in vivo study. *Nanomedicine* **10**, 401–409 (2014).
32. S. J. Shepherd *et al.*, Scalable mRNA and siRNA lipid nanoparticle production using a parallelized microfluidic device. *Nano Lett.* **21**, 5671–5680 (2021), https:/doi.org/10.1021/acs.nanolett.1c01353.
33. P. Valencia, O. Farokhzad, R. Karnik, R. Langer, Microfluidic technologies for accelerating the clinical translation of nanoparticles. *Nat. Nanotechnol.* **7**, 623–629 (2012).
34. R. Mukhopadhyay, When PDMS isn't the best. *Anal. Chem.* **79**, 3249–3253 (2007).
35. H. Cong, N. Zhang, Perspectives in translating microfluidic devices from laboratory prototyping into scale-up production. *Biomicrofluidics* **16**, 021301 (2022).
36. J. Wu, S. Yadavali, D. Lee, D. A. Issadore, Scaling up the throughput of microfluidic droplet-based materials synthesis: A review of recent progress and outlook. *Appl. Phys. Rev.* **8**, 031304 (2021).
37. L. B. Jeffs *et al.*, A scalable, extrusion-free method for efficient liposomal encapsulation of plasmid DNA. *Pharm. Res.* **22**, 362–372 (2005).
38. T. S. Zimmermann *et al.*, RNAi-mediated gene silencing in non-human primates. *Nature* **441**, 111–114 (2006).
39. M. B. Romanowsky, A. R. Abate, A. Rotem, C. Holtze, D. A. Weitz, High throughput production of single core double emulsions in a parallelized microfluidic device. *Lab Chip* **12**, 802–807 (2012).
40. M. Muluneh, D. Issadore, Hybrid soft-lithography/laser machined microchips for the parallel generation of droplets. *Lab Chip* **13**, 4750–4754 (2013).
41. S. Yadavali, H. H. Jeong, D. Lee, D. Issadore, Silicon and glass very large scale microfluidic droplet integration for terascale generation of polymer microparticles. *Nat. Commun.* **9**, 1222 (2018).
42. S. Li *et al.*, Payload distribution and capacity of mRNA lipid nanoparticles. *Nat. Commun.* **13**, 5561 (2022).
43. S. Yadavali, D. Lee, D. Issadore, Robust microfabrication of highly parallelized three-dimensional microfluidics on silicon. *Sci. Rep.* **9**, 1–10 (2019).
44. A. D. Stroock *et al.*, Chaotic mixer for microchannels. *Science* **295**, 647–651 (2002).
45. M. T. Wei *et al.*, Phase behaviour of disordered proteins underlying low density and high permeability of liquid organelles. *Nat. Chem.* **9**, 118–1125 (2017).
46. R. Milo, R. Phillips, *Cell Biology by the Numbers* (Garland Science, ed. 1st, 2015).
47. H. M. Wyss, D. L. Blair, J. F. Morris, H. A. Stone, D. A. Weitz, Mechanism for clogging of microchannels. *Phys. Rev. E Stat. Nonlin. Soft Matter Phys.* **74**, 2–5 (2006).
48. S. S. Massenburg, E. Amstad, D. A. Weitz, Clogging in parallelized tapered microfluidic channels. *Microfluid. Nanofluid.* **20**, 1–5 (2016).
49. R. El-Mayta, M. S. Padilla, M. M. Billingsley, X. Han, M. J. Mitchell, Testing the in vitro and in vivo efficiency of mRNA-lipid nanoparticles formulated by microfluidic mixing. *J. Vis. Exp.* **2023**, 1–14 (2023).
50. D. Laczkó *et al.*, A single immunization with nucleoside-modified mRNA vaccines elicits strong cellular and humoral immune responses against SARS-CoV-2 in mice. *Immunity* **53**, 724–732.e7 (2020).
51. M. G. Alameh *et al.*, Lipid nanoparticles enhance the efficacy of mRNA and protein subunit vaccines by inducing robust T follicular helper cell and humoral responses. *Immunity* **54**, 2877–2892.e7 (2021).
52. H. Yin *et al.*, Therapeutic genome editing by combined viral and non-viral delivery of CRISPR system components in vivo. *Nat. Biotechnol.* **34**, 328–333 (2016).
53. P. P. G. Guimaraes *et al.*, Ionizable lipid nanoparticles encapsulating barcoded mRNA for accelerated in vivo delivery screening. *J. Control. Release* **316**, 404–417 (2019).
54. M. N. Uddin, M. A. Roni, Challenges of storage and stability of mrna-based covid-19 vaccines. *Vaccines* **9**, 1–9 (2021).
55. A. S. Rathore, G. Kapoor, Application of process analytical technology for downstream purification of biotherapeutics. *J. Chem. Technol. Biotechnol.* **90**, 228–236 (2015).
56. S. Streck, L. Hong, B. J. Boyd, A. McDowell, Microfluidics for the production of nanomedicines: Considerations for polymer and lipid-based systems. *Pharm. Nanotechnol.* **7**, 423–443 (2019).
57. S. J. Shepherd *et al.*, Scalable mRNA and siRNA lipid nanoparticle production using a parallelized microfluidic device. *Nano Lett.* **21**, 5671–5680 (2021).
58. M. M. Billingsley *et al.*, Ionizable lipid nanoparticle-mediated mRNA delivery for human CAR T cell engineering. *Nano Lett.* **20**, 1578–1589 (2020).
59. A. Frey, J. Di Canzio, D. Zurakowski, A statistically defined endpoint titer determination method for immunoassays. *J. Immunol. Methods* **221**, 35–41 (1998).